JOINT EUROPEAN TORUS

JET–P(90)33

A. Gibson and JET Team

Fusion Relevant Performance in JET

Fusion Relevant Performance in JET

A. Gibson and JET Team*

JET-Joint Undertaking, Culham Science Centre, OX14 3DB, Abingdon, UK

** See Appendix 1*

Preprint of Paper to be submitted for publication in
Plasma Physics and Controlled Fusion

Fusion Relevant Performance in JET

The JET Team[1]
(Presented by A. Gibson[2])
JET Joint Undertaking, Abingdon, Oxon, OX14 3EA, UK

ABSTRACT

An overview is given of fusion relevant performance in a number of JET operational regimes. It is shown that in most areas JET provides a suitable platform on which to base the design and predict the performance of a next step device. The main outstanding problem area is that of controlling impurity influxes and plasma exhaust, these are to be studied in a new phase programme under consideration for JET. The fusion performance already obtained in JET is described with 100kW of fusion power being generated in charged particles from the D-He^3 reaction and more than 10 MW of fusion power predicted from present discharges if operated in D-T.

1. INTRODUCTION

The Joint European Torus (JET) routinely produces plasmas whose main parameters lie clearly within the reactor regime.

In this paper we describe some of the important reactor relevant properties of these plasmas, especially in the following areas:

(a) Operation near the Density Limit
(b) Operation near the β Limit
(c) The Production of High Temperatures
(d) Confinement Times
(e) Limitations due to Impurity Influxes
(f) Fusion Product Confinement
(g) Fusion Performance

2. OPERATION NEAR THE DENSITY LIMIT

Operation near the density limit has been systematically studied in JET for limiter discharges, with Carbon limiters, with evaporated Beryllium layers and with Beryllium limiters (see Lowry et al, 1990).

The operating density in tokamaks is usually presented in the form given in Fig 1. Each point represents the maximum obtained normalised density during a discharge with either Ohmic (OH), Neutral Beam (NBI), Ion Cyclotron (ICRH) or combined heating. The broken lines marked by OH (C) and NBI(C) are the highest limits obtained in the previous campaigns with Carbon walls and limiters ($nRq/B = 12$ for ohmic heating and 20 with additional heating in units of 10^{19} m^{-3}, m, T). There are clear improvements due to the Be

[1]See Appendix I
[2]Paper prepared by A Gibson and P Smeulders

limiters and Be coated walls, so that nRq/B ~33 is reached with combined heating, ICRH heating and NBI. Furthermore the limiting density increases with the applied power as we shall see shortly. The limit at low q however is unchanged and is still set by major current disruptions. It corresponds to unstable plasma conditions at $q_\psi < 2$ for all densities.

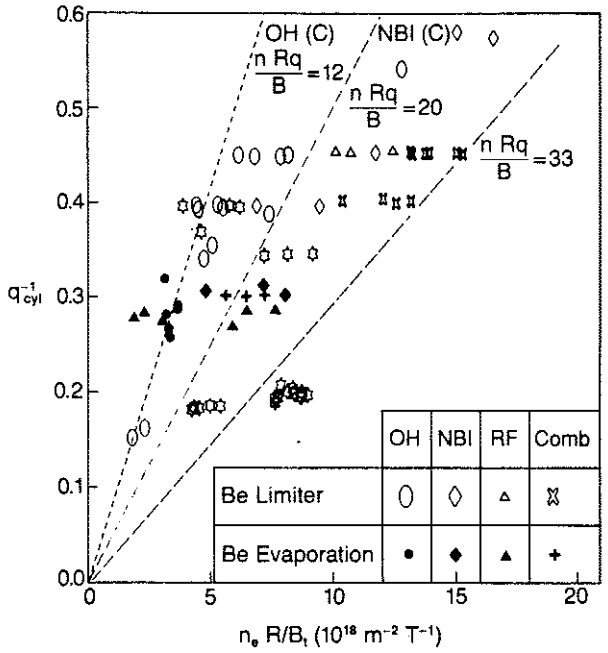

Fig. 1 The operating density range for JET shown as normalised current $q^{-1}_{cyl} = \pi R I_p / 5 A B_\varphi \left[m, MA, m^2, T\right]$ *versus normalised density* $n_e R/B_\varphi$ *[m^{-3}, m, T]. The broken lines with nRq/B = 12 and 20 respectively. represent the maximum density values obtained before the introduction of Beryllium into the vacuum vessel for ohmic heating (OH (C)) and for Neutral Beam heating (NBI (C)). The symbols are the maxima obtained after the introduction of Be for various heating scenarios.*

There has not yet been such a systematic study for X-point discharges, but it is clear that the behaviour is similar, perhaps with somewhat smaller density limits. The highest densities so far in X-point discharge are obtained in H-mode with $\bar{n}Rq_{cyl} / B_t \sim 20 \times 10^{19}$ m^{-2}T^{-1}. At higher densities, typically when $P_{rad}/P_t \sim 60\%$, an H to L-mode transition occurs and the density falls without causing a disruption.

In limiter discharges the nature of the limit is different for C and Be limiters. Whereas with C limiters the limit is marked by a radiative collapse and hard disruption. With Be limiters it is generally marked by the appearance of an asymmetrical edge radiation (MARFE) which, with gas fuelled discharges, is accompanied by a fall in recycling and reduction in density, typically leading to a soft density limit with a relaxation oscillation of density and radiation near the limit. It is also clear that the highest densities are obtained for the points with the highest additional heating. This point is emphasised in Fig. 2.

A number of papers (Gibson, 1976) have suggested that the density limit is determined by a radiation power balance especially in the edge regions of the discharge (Rebut and Green, 1976, Campbell et al, 1986, Wesson et al, 1989). These models suggest that the density limit should increase approximately as $P_t^{1/2}$. Fig 2 shows this type of behaviour for gas and pellet fuelled discharges with Beryllium coated walls.

A number of discharges on Fig. 2 show a MARFE density limit while the other points are existence points where no density limit occured. The MARFE points on this diagram fall in the middle of the existence region. However the MARFE limit for pellet and gas fuelled discharges does lie at the boundary of the existence region if the edge density is used

instead of the line average density. That is MARFE's occur only close to the curve $n_{edge} R/B_t = 2.37\ P^{1/2}$, see Fig. 3.

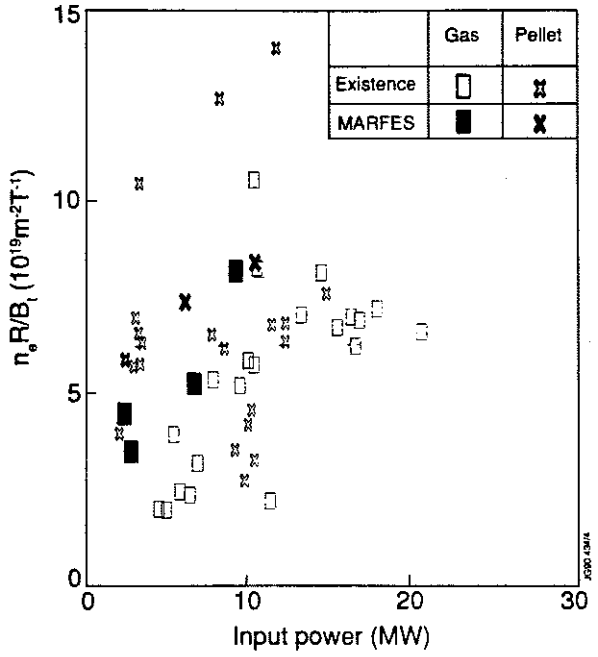

Fig. 2 The normalised line density as function of the input power, the limiting density cases (MARFES) occur throughout the existence region shown in the figure.

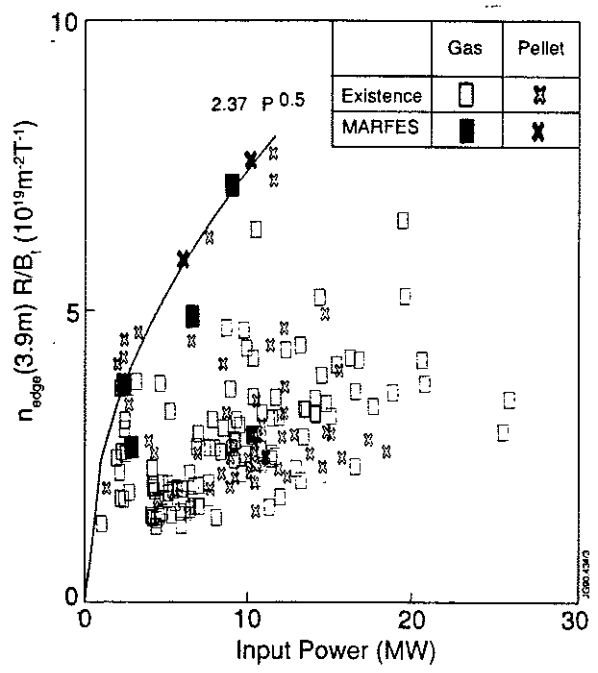

Fig.3 The normalised edge density versus input power showing that the MARFE density limit now occurs at the boundary of the existence region. In this diagram B varies in the range 1.4 to 2.6 T.

Operation near the density limit in JET can thus be summarised as follows :

(a) The density limit for additionally heated discharges in JET, with Beryllium limiters in clean conditions, exceeds $nRq_{cyl}/B_t = 33 \times 10^{19}\ m^{-2}\ T^{-1}$;

(b) The density limit in gas and pellet fuelled discharges increases with input power approximately as $P_t^{1/2}$ and is determined by edge parameters, particularly the edge density;

(c) The radiative nature of the limit and the difference between Carbon and Beryllium walls make it clear that the limit is determined by impurity content and hence wall interaction and material type;

(d) The high value obtained for the limit in JET means that an acceptable limit will be obtained in next step devices provided that a sufficient degree of impurity exclusion can be obtained.

3. OPERATION NEAR THE BETA LIMIT

Troyon established computationally a quantitative estimate for the β limit in tokamaks for reasonable profiles (Troyon et al, 1984) :

$$\beta_{Troy} = 2.8 \times 10^{-2} I_p / B_\varphi a \text{ (MA, T, m)} \qquad (2.1)$$

Many experiments have shown steady state high β operation close to this limit and even at somewhat higher values. (ASDEX, Ryter et al, 1990; DIII-D, Ferron et al, 1990; PBX, Takahashi et al, 1990)

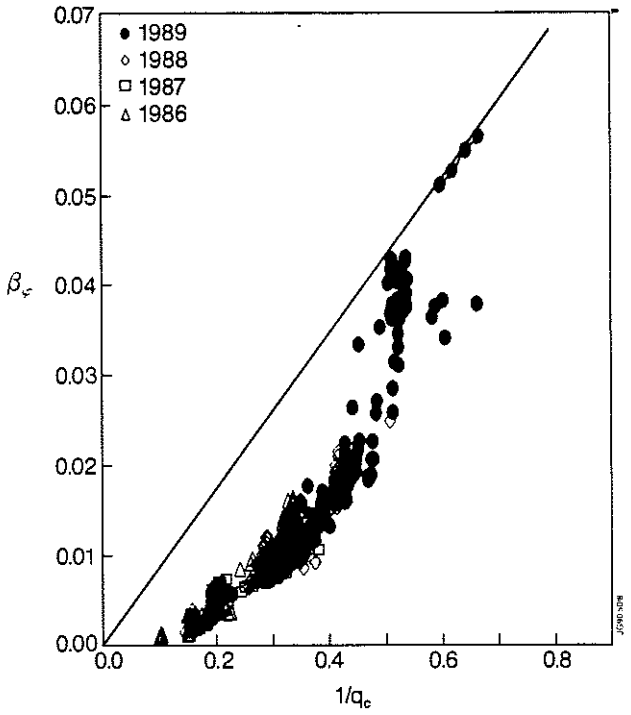

Fig. 4 The maximum toroidal beta ($\beta_\varphi = 2\mu_0 \langle p \rangle / B_\varphi^2$) as function of the normalised current $q_{cyl}^{-1} = \pi R I_p / 5 A B_\varphi$ for all JET discharges from 1986-1989 with the poloidal beta $\beta_\varphi > 0.4$. The line is approximately the Troyon limit, $\beta_{Troyon} = 0.028\, I_p/aB_\varphi$ [MA,m,T]. The highest β of 5.5% is obtained in a 2 MA, Double-Null H-mode discharge at 0.9T with $T_e(0)$=3.7 keV, $T_i(0)$ =6.3 keV, $n_e(0) = 3 \times 10^{19} m^{-3}$, τ_E = 0.35 s, q_{cyl} = 1.6, q_ψ = 2.2, P_{NB} = 11 MW, 80 kV D-injection in a H-plasma.

In JET, the Troyon limit has been reached within the available heating power at reduced toroidal field in Double Null H-mode discharges. (Smeulders et al, 1990). Fig. 4 shows for a number of JET discharges the maximum β obtained as a function of q_c^{-1}. Values within a factor of two of the Troyon value are readily obtained and the highest values reach the Troyon limit.

These values were obtained for a discharge where the toroidal magnetic field was lowered from 1.1 to 0.9T at a constant neutral beam (NB) power of 11 MW while the β remained close to the Troyon value limit as shown in Fig. 5. The discharge is already sawtoothing before the β limit is reached. NBI is switched on progressively from t = 13s, β increases

progressively until Troyon limit is reached at t = 14.3s. The β value then falls from the limit value by ~10% at each sawtooth crash and climbs back between the crashes.

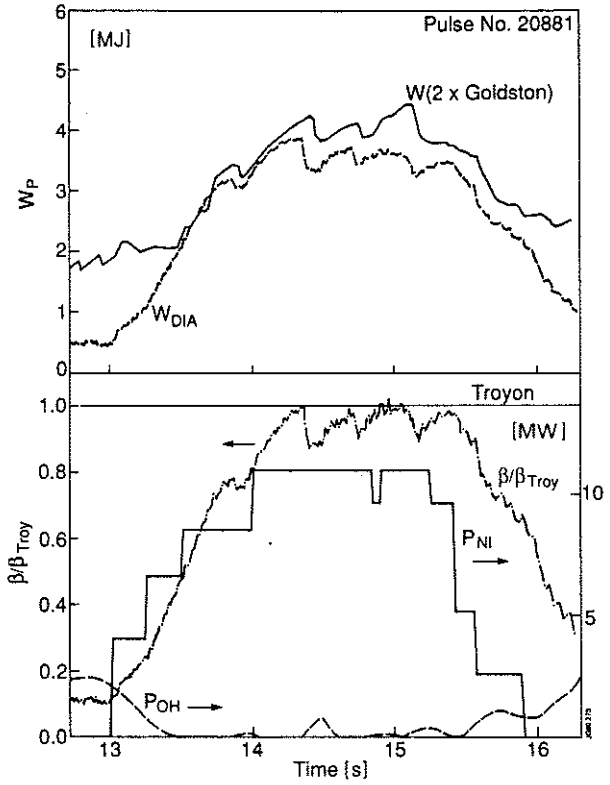

Fig. 5 The observed plasma energy W_{DIA} and the energy W_G calculated from the effective input power (P_t–dW/dt) and $\tau_E = 2\tau_G$ for the highest beta discharge as a function of time. Also shown are the normalised beta β/β_{Troy}, NBI and OH powers.

This discharge like other H-mode discharges in JET has $\tau_E \sim 2 \times \tau_G$ (Eq. 4.1). Fig. 5 also shows the observed plasma energy W_{DIA} and the energy W_G calculated from the power input and $\tau_E = 2x\tau_G$. When the β limit is reached W_{DIA} is close to or below W_G This could be because the confinement time has degraded to give a soft limit, or it could be because the power applied in this discharge is only just enough to reach the limit. Clearly an important experiment to do in JET is to increase the input power significantly above the value needed to reach β_{Troy} and see whether the confinement time does indeed degrade to maintain a soft limit.

4. CONFINEMENT TIMES

The confinement time in JET discharges generally degrades with increasing power flow through the plasma. An example for H-Mode discharges is shown in Fig. 6. The energy confinement time is defined in the usual way as $\tau_E = W/(P_t - dW/dt)$, where P_t is the total power input to the plasma and W is the plasma kinetic energy content (usually measured by a diamagnetic loop). The experimental values roughly follow a scaling of the Goldston type (Goldston et al, 1984) with a multiplier, H of ~2 :

$$\tau_E(G) = 3.7 \times 10^{-2} H I_p \left(P_t - [dW/dt]\right)^{-0.5} R^{1.38} (a/R)^{-0.37} (b/a)^{0.5} \quad (MA, MW, m) \qquad (4.1)$$

It should be noted that for a power-flow of 10 MW the energy confinement time can reach ~1 s and for 20 MW can exceed ~0.5 s.

The inclusion of the (dW/dt) term in the definition of τ_E(G) permits the inclusion on Fig. 6 of a number of data which have not reached steady state. However more than 90% of the

data have (dW/dt) < 0.5 P_t and more than 60% have (dW/dt) < 0.3 P_t. The term (dW/dt) thus always has the nature of a correction but it does significantly improve the fit to the scaling relation.

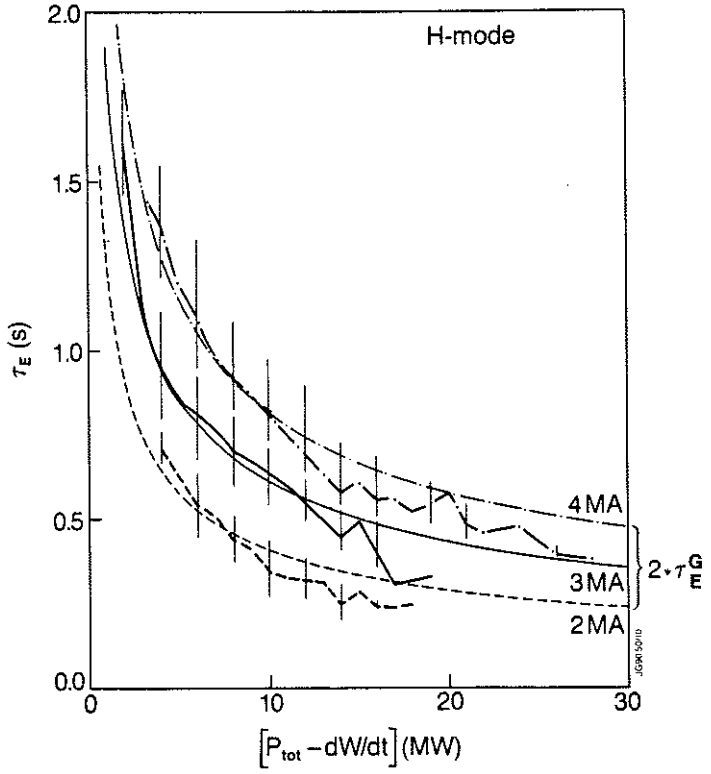

Fig. 6 Energy confinement time τ_E as a function of the effective input power $P_{eff} = (P_{tot} - dW/dt)$ for H-mode plasmas with currents of 2,3 and 4 MA. The smooth curves are twice the Goldston scaling for each current. The bars represent the scatter of the experimental data (being ± one standard deviation).

5. THE PRODUCTION OF HIGH TEMPERATURES

The observed confinement time τ_E and the available power P_t limit the plasma energy that can be obtained. Thus for a JET H-mode discharge at 4 MA with an input power around 20MW and a confinement $\tau_E \sim 0.5$ s, the average temperature <T> would be around 6keV at average densities around $3 \times 10^{19} m^{-3}$. Consequently strong temperature profile peaking of $(T_i(0)/<T>) \geq 5$ is required to get the central temperatures of ~30 keV which are of fusion interest.

Such strong temperature profile peaking factors are indeed observed for the ion temperatures in low density discharges. Central ion temperatures $T_i(0)$ of 28 keV have been obtained at high power levels per particle as shown in Fig. 7(a). Note that there is a steady increase in $T_i(0)$ with increasing $P_t/<n>$, but also a large spread. Thus the highest $T_i(0)$ values are obtained for $P_t/<n>$ in the range 5 - 10 while for $P_t/<n> = 5$, $T_i(0)$ ranges from 12 to 28keV. The quantity $P_t/<n>$ is thus an indicator rather than a true scale parameter. The high $T_i(0)$ values are associated with a progressive increase in the peaking factor $(T_i(0)/<T>)$ which reaches a value of 6 for those values of $P_t/<n>$ that have the highest $T_i(0)$ values (see Fig. 7(b)).

The slope of the increase of $T_i(0)$ with $P_t/<n>$ represents a central confinement time and the fact that $T_i(0)$ increases roughly linearly with $P_t/<n>$ means that the energy confinement of the ions in the plasma centre does not degrade with $P_t/<n>$. The same is not true for the electrons as can be seen in Fig. 7(c). There is a strong saturation at $T_e(0)$ of around 8keV implying a strong decrease in the central electron confinement time as $P_t/<n>$ increases.

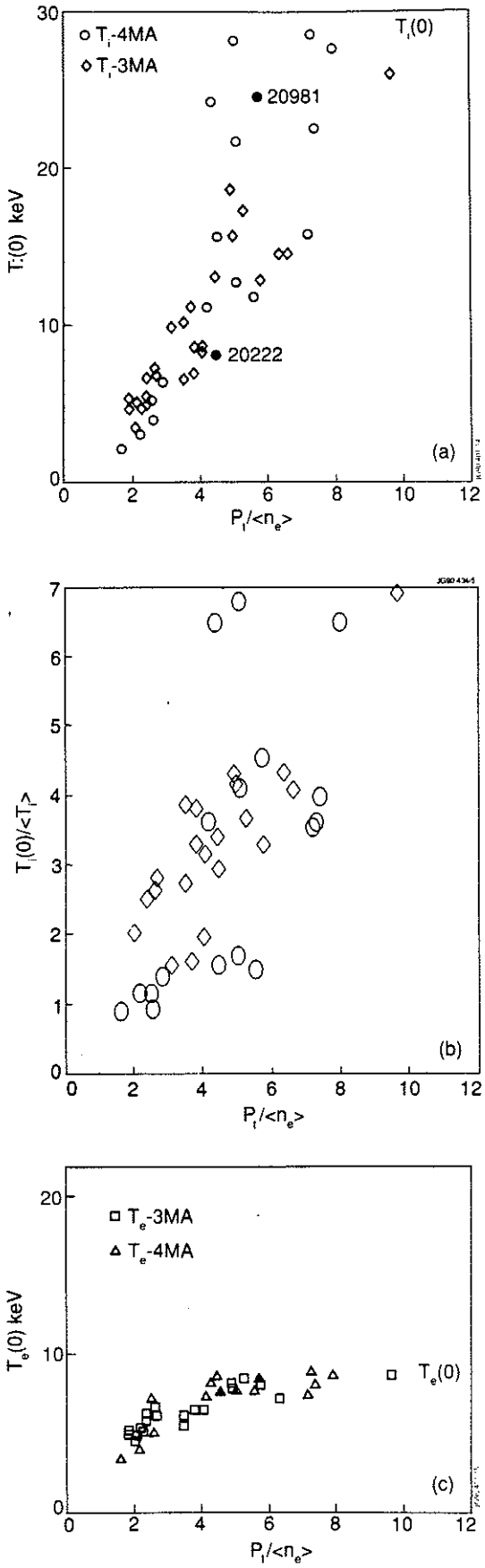

Fig. 7 (a) The dependence of the highest central ion temperature $T_i(0)$ reached in each pulse on the ratio of the total input power P_t to the averaged electron density $\langle n_e \rangle$, at the same time, for 3 MA (□,◊) and 4 MA (o,Δ) H-mode discharges with NBI heating and gas fuelling.
(b) The temperature profile peaking factor $T_i(0)/\langle T_i \rangle$ versus $P_t/\langle n_e \rangle$ for the same discharges.
(c) The central electron temperature $T_e(0)$ versus $P_t/\langle n_e \rangle$.

Of course it has to be remembered that rather little power goes to the electrons in these discharges. In the central region (~a/3), typically 90% of the neutral beam power goes to the ions. Nevertheless there is a marked difference in behaviour between the $T_i(0)$ and $T_e(0)$ in going between the indicated Pulse Nos: 20222 and 20981, as shown in Table. I. Both pulses have I_p = 4MA, B = 2.8T, but for Pulse No: 20222 the applied NB power has mainly 80kV acceleration (13.8 MW at 80 kV; 1.8 MW at 140 kV), whereas Pulse No: 20981 has appreciable power with 140 kV acceleration (12.1 MW at 80 kV; 5.8 MW at 140 kV).

Table I

Parameters	Pulse No: 20222 (t = 9.9 s)	Pulse No: 20981 (t = 11.4 s)	Units
$\hat{P}_i$ (r<a/3)	3.5	4.5	MW
$\hat{P}_i/\hat{n}$	0.6	1.1	10^{-19} MW m^3
$T_i(0)$	8	22	keV
$\hat{P}_e$(r<a/3)	0.7	1.5	MW
$\hat{P}_e/\hat{n}$	0.1	0.4	10^{-19} MW m^3
$T_e(0)$	8	9	keV
$\hat{n}_e$	6	4	10^{19} m^{-3}

A change of a factor of about 2 in the ion input power per particle $P_t/\langle n\rangle$ leads to a large change in $T_i(0)$ presumably because the ion losses do not increase with P_t. For the electrons the situation is less clear due to the low power given to them, consequently there are large errors in the electron power balance. Nevertheless the $P_t/\langle n\rangle$ changes appreciably (estimated to be by about a factor of 4) without a significant change in $T_e(0)$ presumably because of a strong degradation of the electron confinement time with power.

A more precise analysis of the energy balance in the central region of these discharges was not possible because of the difficulty in obtaining sufficiently accurate data on temperature and deposition profiles.

Electron Heating

Ion cyclotron resonance heating produces energetic (MeV) ions in the plasma and by this means, in contrast to neutral beams,primarily heats the electrons (typically > 90% of ICRH power goes to the electrons). An obvious next step is to apply centrally deposited ICRH power to the hot ion discharges described above in order to attempt to increase the central T_e which is important in order to get reactor like plasmas with $T_e(0) \sim T_i(0)$.

The introduction of Be antenna screens has solved previous ICRF heating impurity production problems. Consequently effective ICRF electron heating is now possible in both limiter and H-mode discharges. Electron temperatures as high as 12 keV have been obtained. However, initial experiments in limiter configuration (Lomas, et al, 1990) show saturation at this value as $P_{ICRF}(0)/n_e$ is increased above 2 x 10^{19} MW m^3. Further experiments are required in order to establish whether this saturation is due to transport or possibly a difference in the deposition profile.

High temperature operation in JET can thus be summarised, as follows:

(a) Application of high power beam and ICRF heating to JET has produced

$T_i(0)$ > 28 keV

$T_e(0)$ > 12 keV

Discharges have been produced in which $T_i(0)$ and $T_e(0)$ are simultaneously in excess of 10keV.

(b) Experiments to use ICRF heating to heat the electrons in the present hot ion discharges have begun, but need further development.

6. LIMITATIONS DUE TO IMPURITY FLUXES

The highest performance conditions in JET are obtained in X-point and H-mode discharges. The duration of these conditions is limited to ~ 1s or less by a large influx of Carbon impurity released from local hot spots which form on the X-point dump plates (carbon-carbon fibre composite). A similar behaviour occurs for discharges limited on the inner wall of JET.

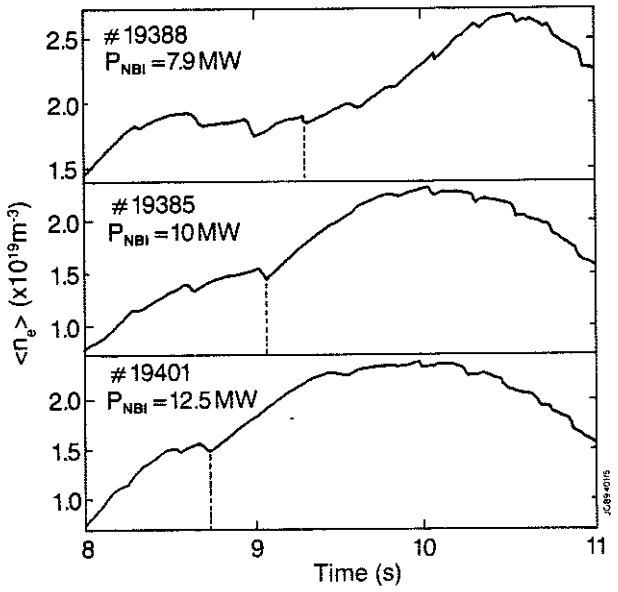

Fig. 8 Effect of varying the additional heating power P on the onset of the high carbon influx. The onset is readily visible on the line average electron density $<n_e>$ for the Pulse Nos: 19388, 19385, and 19401, it is marked by the vertical broken lines. The product P.t(onset) is about 10 MJ : the higher the heating power the shorter the time delay for the carbon influx.

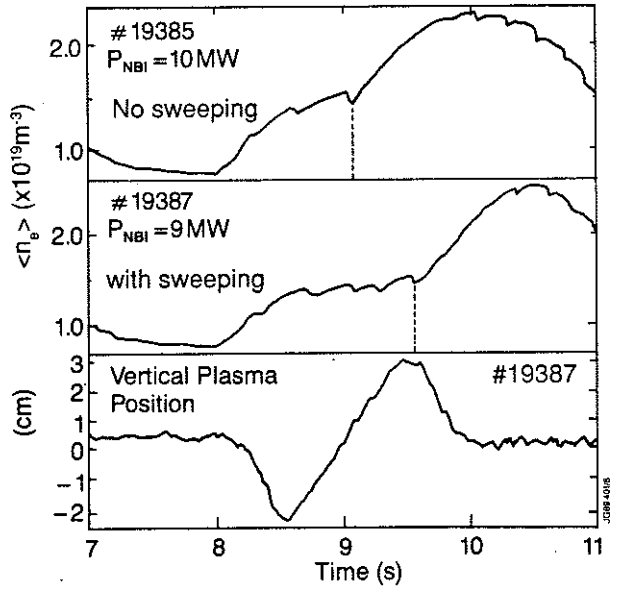

Fig. 9 The dependence of the onset of the carbon influx on the sweeping of the plasma contact position on the inner wall limiter. Comparison of a discharge Pulse No: 19385 without and with sweeping Pulse No:19387. Sweeping of the plasma on the inner wall delays the carbon influx by a few hundreds of ms.

Measurements by Pasini et al (1989) in Figs. 8 and 9 show this effect. In Fig. 8, n_e is given as a function of time for 3 shots with different power levels. The sharp increase in n_e is a direct indication of the carbon influx. The onset of the influx can be delayed by sweeping the position of the plasma-wall contact over the carbon tiles, so that a wider distribution of

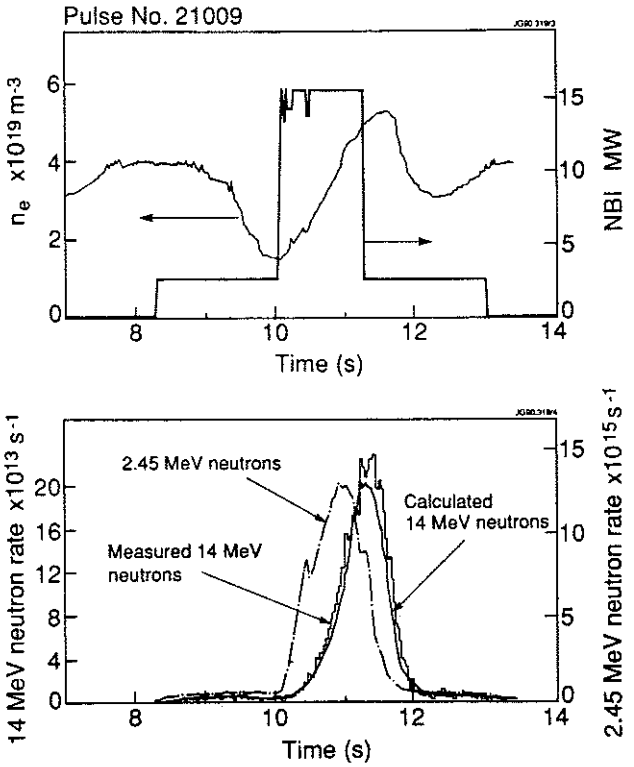

Fig. 10 The upper part shows the time evolution of the electron density $<n_e>$ and that of the NBI power. In the lower part the measured 2.45 MeV neutron (originating from D-D reactions) and the 14 MeV neutron (coming from D-T reactions) rates are shown. Also shown is the calculated neutron rate by the D-T reactions resulting from the tritons produced by the D-D reactions and an assumed triton loss time of 2s.

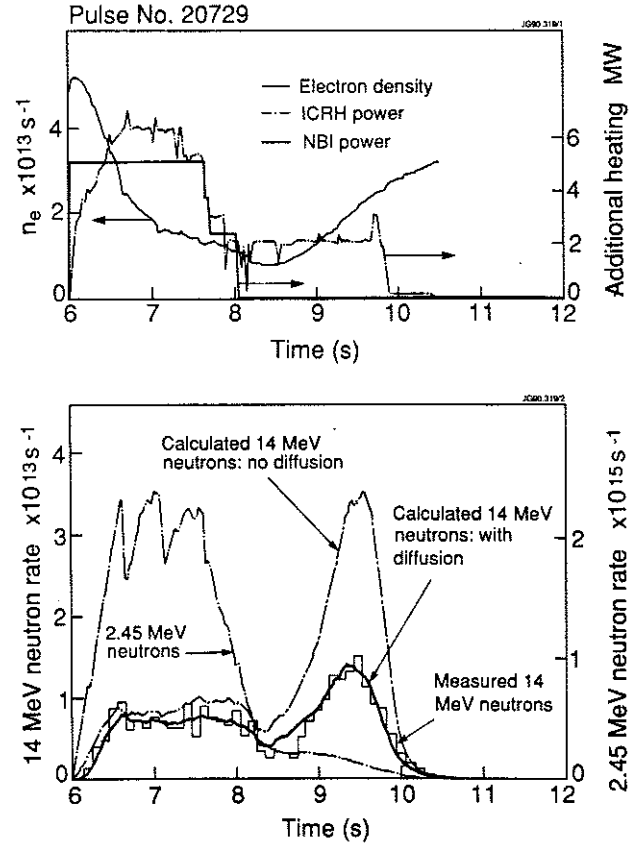

Fig. 11 The upper figure gives the NBI and ICRH powers versus time together with the electron density $<n_e>$. In the lower half the measured 2.45 and 14 MeV neutron rates are given as a function of time. Also shown are calculated 14 MeV neutron emission rates with and without the triton diffusion model.

the heat over the tiles occurs. In Fig. 9, this can be seen for Pulse No: 19387, for which the vertical position has been changed from -2 to +3 cm thus sweeping the interaction area and giving an extra delay of around 0.5 s. This demonstrates that if one can devise an X-point target chamber, which can accept the heat flux without excessive wall temperatures the plasma can be kept clean and undiluted. This excessive wall loading behaviour which limits the performance of JET is a serious problem which must be overcome before a long burn ignition experiment can be designed.

A new phase program has been formulated for JET to address this problem using an internal pumped divertor with a radiating plasma channel to spread the heat load, impurities are expected to be kept away from the main discharge by plasma flow along the channel.

7. CONFINEMENT OF FUSION PRODUCTS

The slowing down and confinement behaviour of 1 MeV tritons generated in D-D fusion reactions in JET has been studied by comparing the 2.45 MeV neutron emission, which has the same time profile as the triton generation, with the 14 MeV neutron emission emitted as the tritons slow down to the peak D-T reactivity energy of 0.18 MeV (Conroy et al,1990). The observed time profile of 14 MeV emission is compared with that calculated from a multi-group test particle, slowing down model. The model includes a diffusive loss mechanism which can also be represented by a simpler exponential loss time applied to each group.

For a typical JET discharge (4MA, X-point with NBI), the classical triton slowing down time is ~0.7s and the model gives a good fit to the observations with a triton loss time of about 2s (determined by the quality of the fit). An example is shown in Fig.10, which also shows the NBI power and the central electron density n_e as a function of time.

The triton confinement time can be determined more accurately in certain extreme discharges with high T_e (~ 7keV) and low n_e ($\sim 10^{19}$ m^{-3}), and hence long triton slowing times (>2s), as shown in Fig. 11. A good agreement between the calculated and measured 14 MeV neutron rate can only be obtained if a diffusive transport of D = 0.1 $\pm$ 0.05 m^2s^{-1} is included, this is also modelled by an exponential loss time of τ= 2 s.

Alpha-Particle Simulation

High energy (several MeV) minority ions (H and He^3 in D plasma) generated by ICRH in JET provide a good simulation for the behaviour of α-particles to be expected in the D-T phase of JET and in a reactor. In some JET discharges, the energy in these fast particles can reach 50% of the total plasma energy.

When the minority species is He^3 in a D plasma the fusion power generation can be large. In fact the largest fusion power so far generated in JET comes from this process. In recent experiments using Beryllium coated walls to reduce the dilution of deuterium by impurities this power has reached 100 kW, as shown in Fig. 12 which shows D-He^3 fusion power as a function of ICRH heating power. Also shown are the results for JET with carbon walls published previously (Boyd et al, 1989). The increased D-He^3 fusion power from 60 to 100 kW reflects the improvement of n_D/n_e due to be Be walls.

A comparison of plasma and α-particle (He^3) parameters measured in JET and those for the future D-T operation and for an ignited next step are given in Table II (Bickerton, 1988). The only major difference between the parameters in the α-particle simulation experiments in JET and those foreseen for the future lies in the large velocity space anisotropy of the high energy He^3 particles generated by the ICRF heating.

Slowing Down and Loss Behaviour of Fast Particles

Start et al (1990) describe a model calculation of the energy content of the fast ions in these minority heating experiments. The model includes classical slowing down of the fast ions

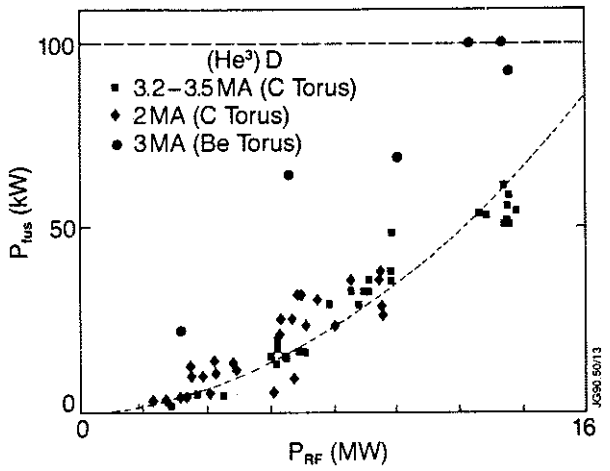

Fig. 12 The measured fusion production P_{fus} in a deuterium plasma with He^3 minority as function of the ICRH power P_{RF}. The solid symbols (■,◆) are the fusion yields in a carbon vacuum vessel. The higher points (•) are obtained after the introduction of Be and reflect the improvement of n_D/n_e from < 0.6 to > 0.8 and correspond to Q (D-He^3) ~ 7 x 10^{-3} at the highest powers.

Table II: Fast or Alpha-Particle Parameters

Parameter	Achieved on JET	Expected Values JET Q=1	Ignited ITER
n_{fast} / n_{eo}	(1-3)%	0.1%	0.7%
$<E_{fast}>$	(1-5) MeV	2 MeV	2 MeV
$<\beta_{fast}>$	0.8%	0.6%	2%
$<p_\perp / p_{//}>$	10-50 (calculated) >7 (measured)	1	1
ρ_θ / a	0.3 (2MA)	0.3 (5MA)	0.07 (20MA)
v_{fast}/v_A	2 - 4 $_\perp$	2	2.8
τ_{sd}/τ_E	≈1	≈1	0.2 - 1

on the plasma, taking into account the finite orbit size and the variation of slowing time over the orbit.

Fig. 13 compares the measured with the calculated fast particle energy, for various discharges, which were centrally heated with no sawteeth. Fig. 13(b) shows the results with finite orbit width included in the calculations, Fig. 13(a) has no orbit width included. It can be seen that the model gives a good fit to the observed fast ion content when orbit effects are included, without the need to introduce any extra fast ion loss term.

If nevertheless such a term is introduced into the model, Cottrell (1990) has shown that the fit becomes noticeably worse if τ_{loss} <2s (equivalent to D~ $a^2/4\tau$ > 0.1 m^2s^{-1}), as can be seen in Fig. 13(c). This is in good agreement with loss times deduced from Triton slowing down observations discussed above. Furthermore the loss time for the α particles corresponding to D_α ~ 0.1 m^2s^{-1} is comparable to typical plasma diffusion coefficients estimated in the core of similar JET plasmas which are in the range of 0.05 to 0.25 m^2s^{-1}. The loss times of about 2s are adequately long enough for the α-particles in a reactor plasma to give their energy to the plasma.

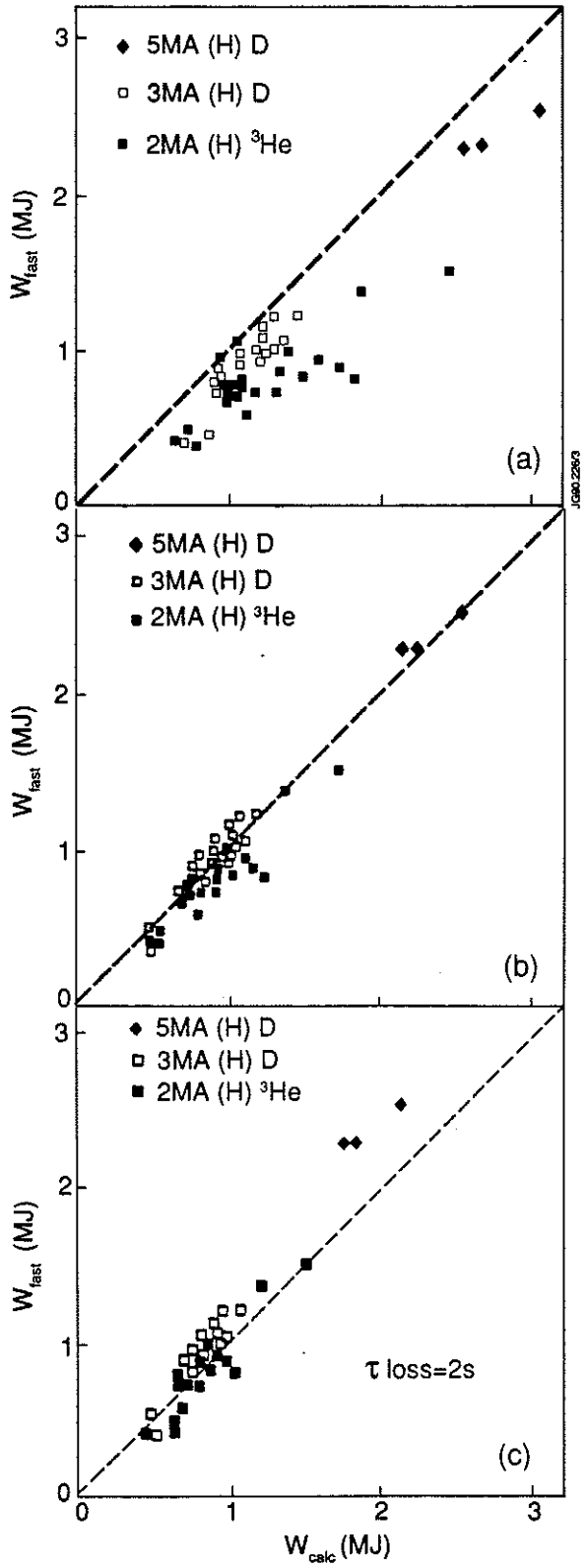

Fig. 13 Measured fast H-ion energy for D and He^3 plasmas versus calculated fast ion energy for a zero-orbit-width model (Fig. 13a) and for a finite orbit-width model (Fig. 13(b)), and with the inclusion of τ_{loss} = 2s (Fig. 13(c)). The fit in Fig. 13(c) is noticeably worse than in Fig. 13(b). τ_{loss} > 2 s implies that D_{fast} ($=a^2/4\tau_{loss}$) < 0.1 m^2/s.

8. FUSION PERFORMANCE IN JET

The fusion performance obtained in JET is shown in Fig. 14. The product $(n_D(0)T_i(0)\tau_E)$ is shown as a function of $T_i(0)$ for various plasma currents in H-modes, pellet and low density high $T_i(0)$ discharges. The points on the diagram are observed values in JET. The curves are values of P_α/P_{loss} for a thermal 50:50 D-T plasma. The shaded bands represent

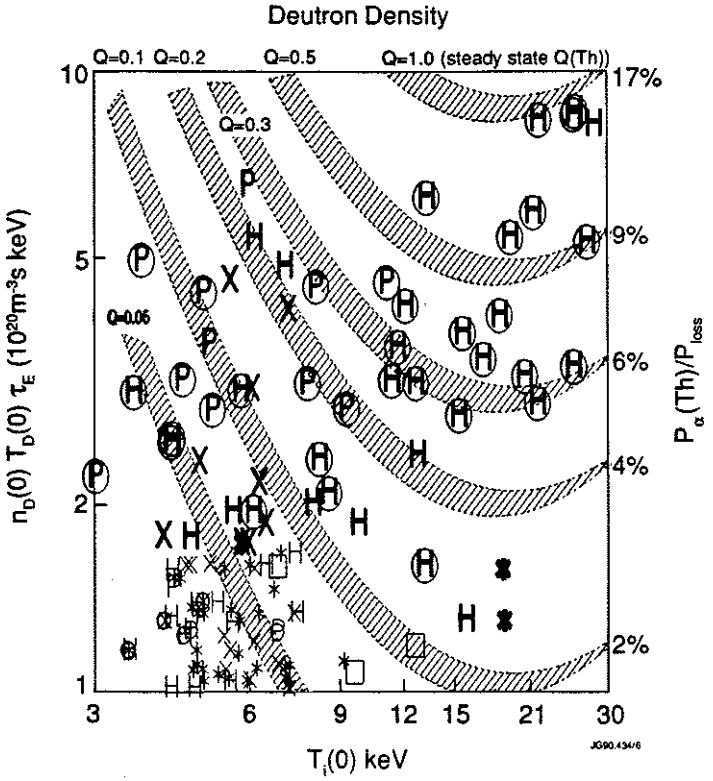

Fig. 14 The product of $(n_DT_i(0)\tau_E)$ as a function of $T_i(0)$ for I_p between 2 and 6.5 MA in H-modes (H), pellet (x), H-modes with pellets (P), and other discharges (*). The experimental points are averaged over 0.2s. Also indicated in the graph are shaded bands of constant P_α/P_{Loss} for a thermal 50:50 D-T plasma. In steady state these bands also correspond to the Q_{DT} shown. The width of the bands covers a range of profiles $\sim[1-(r/a)^2]^\alpha$ and dilutions in the case from $\alpha_n = 0.5$, $\alpha_T = 1.5$ with $n_D/n_e = 1$ to $\alpha_n = 0$, $\alpha_T = 1.3$ with $n_D/n_e = 0.8$ and the addition of a 20% temperature pedestal. It will be seen that the Q values especially at higher $T_i(0)$ are insensitive to these variations. The encircled points are in non-steady state with $(dW/dt)/P_t > 0.3$. For these points the shaded bands represent the thermal component of P_α/P_{Loss}, but not of course the thermal Q.

the effect of reasonable profile and Z_{eff} variation. The Q values[3] indicated are values which would apply to a steady-state thermal plasma (50:50 D-T) with same $(n_DT_i\tau_E)$, i.e. the value to be expected if P_t was reduced until $(dW/dt) = 0$. The actual Q for the highest JET points, which are not in steady state, is about half the value indicated by the curves.

Note that the $(n_DT_i\tau_E)$ values plotted include fast injected particles and thus show what $(n_DT_i\tau_E)$ the configuration could sustain. The thermal $((n_DT_i\tau_E), T)$ for the highest point is roughly 40% lower than the total value. Note also, that the best discharges are 4MA H-modes; (5MA H-mode discharges are not yet optimised). High current (<5 MA) limiter discharges with pellet peaking, sawtooth suppression and combined heating are also making substantial progress in the fusion product.

Other discharges e.g. ICRH H-modes and combined heating H-modes reach appreciable $((n_DT_i\tau_E)$, T) values : (2.5×10^{20} , 4 keV) and (3×10^{20}, 9 keV) respectively. The highest $(n_DT_i\tau_E)$ values of $\sim 9 \times 10^{20}\ m^{-3}$keVs approach those,that are required for Q=1 in a steady-state 50 : 50 D-T plasma.

---

[3] Q is the ratio of the total fusion power (α-particles and neutrons) over the total power input for a plasma in steady state.

The actual fusion power measured in these D plasmas is shown in the form of the Q_{DD} versus volume averaged density in Fig. 15. The highest Q_{DD} values are obtained at moderate densities and high ion temperatures in H-modes. The highest H-mode values are twice those in L-mode. The highest Q_{DD} values have similar contributions from thermal and from beam-plasma processes.

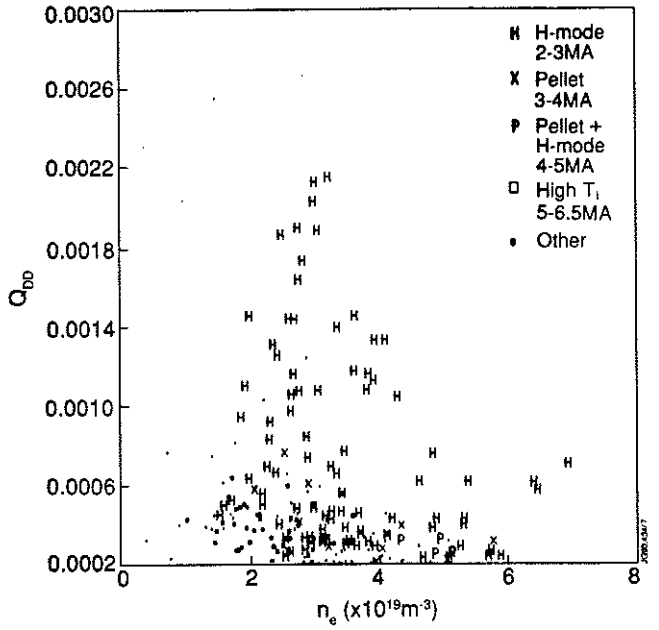

Fig. 15 Measured Q_{DD} values averaged over 0.2 s as function of the volume averaged electron density $<n_e>$ with the same designations as in Fig. 14.

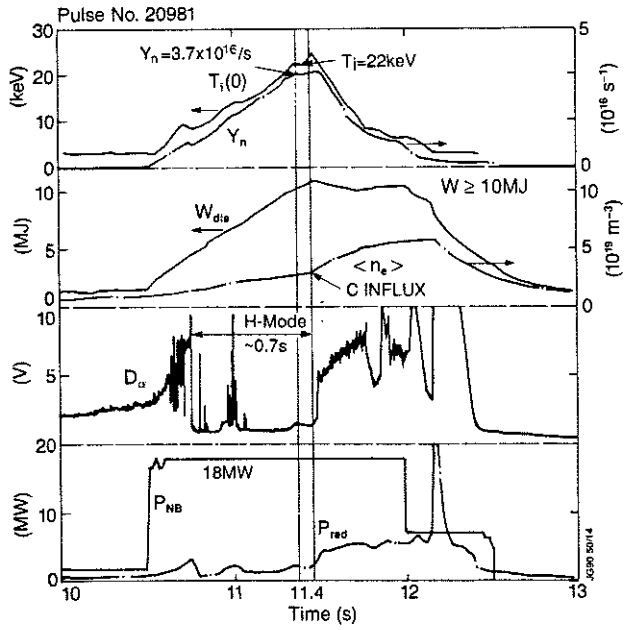

Fig. 16 Time evolution of high fusion yield H-mode Pulse No: 20981. From top to bottom are depicted the central ion temperature $T_i(0)$, the total neutron yield Y_n, the plasma diamagnetic energy W_{dia}, the volume averaged electron density $<n_e>$ and D_α intensity near the X-point, the neutral beam power P_{NB} and the radiated power losses P_{rad} as function of time. The large carbon influx at 11.5 s (marked by the second vertical line) is followed by a termination of the H-mode and an abrupt decrease in the high values of the fusion relevant parameters.

The time evolution of a discharge with such high Q_{DD} values is shown in Fig. 16. The top traces show the time development of a central ion temperature together with the neutron yield. Also shown are the total plasma energy as measured by the plasma diamagnetism and the volume averaged density. The break in the slopes of T_i, T_n, W_{dia}, $\langle n_e \rangle$ in time, mark the point where the carbon influx becomes important shortly before 11.5 s. The X-point discharge is in a H-mode state over nearly 1 s, as can be seen from the D_α signal. The bottom traces are the total NB power and the radiation losses measured in time. Despite the large carbon influx, radiation losses never become dominant in this discharge. The main fusion relevant parameters for this Pulse No: 20981 are summarised in Table III, at t=11.4s.

The relevant fusion parameters calculated by the TRANSP Code for 140 keV NBI of D beams into a T plasma are shown in Table IV. The data are calculated for a discharge otherwise similar to Pulse No: 20981 and are also in non-steady state.

Table III: Double Null H-mode
Pulse No:20981 (t=11.4s)

Plasma Parameters

$T_i(0) = 22keV$	$\bar{T}_i = 5.8keV$
$T_e(0) = 8.6keV$	$\bar{T}_e = 5.2keV$
$W_p = 10MJ$	$dW_p/dt = 8.9MW$
$n_0(0) = 3.7x10^{19}m^{-3}$	$\bar{n}_D = 3.2x10^{19}m^{-3}$
$n_D(0)/n_e(0) = 0.9$	$\bar{n}_D/\bar{n}_e = 0.8$
$Z_{eff}(0) = 1.4$	$\bar{Z}_{eff} = 1.9$
$P_{in} = 18MW$	$\tau_E = 1.1s$
$\beta = 1.8\%$	$\beta/\beta_{Troyon} = 0.5$

Neutron Rate $= 3.5x10^{16}ns^{-1}$

D-D Observed Fusion Parameters

$Q_{DD} = 2.0x10^{-3}(>1.4x10^{-3}$ for $\sim 0.5s)$

$P_{fus} = 43kW\ (D-D)$

$n_D(0)T_D(0)\tau_E = 9x10^{20}m^{-3}keV\,s \quad (>3x10^{20}$ for $\sim 0.5s)$

Table IV: Double Null H-mode
Pulse No. 20981

Equivalent D-T Parameters

Calculated (TRANSP Code) for 140kV injection of D beams into a T target (leading to T:D=2:1)

Q_{DT}	= 0.7	(>0.5 for ~0.8s)
$Q_{thermal}$	= 0.13	
$Q_{beam\text{-}plasma}$	= 0.57	
P_{fuse}	= 12MW	(>8MW for ~0.8s)
P_α	= 2.4MW	(>1.6MW for ~0.8s)
P_α/P_{loss}	= 23%	(>15% for ~0.8s)

9. CONCLUSIONS

JET plasmas now display most of the characteristics to be expected from a reactor plasma:

- Densities up to $\bar{n}Rq_{cyl} / B_t = 33\ m^{-2}T^{-1}$ with $\bar{n} = 1.4 \times 10^{20}\ m^{-3}$ are obtained and appear to be limited by edge radiation loss processes.

- β values up to 5.5 % equal to the Troyon limit value at $B_t = 0.9$ T are obtained

- Strongly peaked ion temperatures > 28 keV with $T_i(0) / \bar{T}_i \sim 6$ are obtained in low density H-mode discharges.$T_i(0)$ and $T_e(0)$ are simultaneously in excess of 10 keV in higher density discharges

- Energetic (MeV) particles both with isotropic and with transverse velocities are contained for at least 2s while they slow down by apparently classical processes. This is adequately long enough for energy transfer in a reacting plasma, where even better confinement should be expected given the increased size and plasma current.

- The duration of fusion relevant conditions in JET H-mode discharges is at present limited to ≤ 1s by the influx of carbon impurities from localised plasma-target plate interaction. A new phase for JET is planned to develop a reactor relevant solution to this problem

- **100 kW** of fusion power in charged particles has been produced in D(He^3) plasmas. $\mathbf{n_D(0)T_i(0)\tau_E}$ values of **7 to 9 x 10^{20} m^{-3}keVs** with $\mathbf{Q_{DD} > 2 \times 10^{-3}}$ have been produced in D-D plasmas. For the same plasma parameters in a D-T plasma this is equivalent to $\mathbf{Q_{DT} \sim 0.7}$, $\mathbf{P_\alpha \sim 2.4\ MW}$, $\mathbf{P_{fusion} \sim 12\ MW}$ with $\mathbf{P_\alpha/P_{Loss} > 20\%}$.

REFERENCES

Bickerton, RJ et al, (1988) Proc. 12th Int. Conf. on Plasma Phys. and Contr. Nucl. Fusion Research, Nice, Nuclear Fusion Supp 1989

Boyd, DA et al, (1989) Nuclear Fusion **29**(1989) 593

Campbell, DJ et al, (1986) Proc. 11th Int. Conf. or Plasma Physics and Contr. Nucl. Fusion Research, Kyoto, Nuclear Fusion Supp. 1987.

Conroy, S et al, (1990) Europhysics Conf. Abstracts **14B**, 98 (1990)

Ferron, J et al, (1990) Europhysics Conf. Abstracts **14B**, 371(1990)

Gibson, A, (1976) Nuclear Fusion, **16** (1976) 546

Goldston, RJ et al, (1984) Plasma Physics and Controlled Fusion **26**, 87 (1984)

Lomas, PJ et al, (1990) Europhysics Conf. Abstracts **14B**, 5 (1990)

Lowry, C. et al, (1990) Europhysics Conf. Abstracts **14B**, 338 (1990)

Pasini, D et al, (1989) "Observations on the Erosion of Carbon at High Temperatures in JET", Topical Meeting on High Temperature Erosion of Graphite in Plasmas, Princeton Plasma Physics Laboratory, July 25-27, 1989. To be published as a DOE report on Plasma Material Interaction and High Heat Flux Test Group.

Rebut, P-H, and Green, BJ Plasma (1976) Proc. 6th Int. Conf. on Plasma Phys. and Contr. Nucl. Fusion Research, Berchtesgaden, Nuclear Fusion Supp 1977

Ryter, F et al, (1990) Europhysics Conf. Abstracts **14B**, 94 (1990)

Smeulders, P et al, (1990) Europhysics Conf. Abstracts **14B**, 323 (1990)

Start, DF et al, (1990) Europhysics Conf. Abstracts **14B**, 1015 (1990)

Takahashi, H et al, (1990) Europhysics Conf. Abstracts **14B**, 367 (1990)

Troyon, F et al (1984), Plasma Physics and Controlled Fusion **26**, 209 (1984)

Wesson, JA et al, (1989) Nuclear Fusion, **29** (1989) 641

APPENDIX I

THE JET TEAM

JET Joint Undertaking, Abingdon, Oxon, OX14 3EA, U.K.

J.M. Adams[1], H. Altmann, A. Anderson[14], S. Attenberger[23], W. Bailey, P. Ballantyne, B. Balet, R. Barnsley[29], D.V. Bartlett, L.R. Baylor[33], A.C. Bell, P. Bertoldi, E. Bertolini, V. Bhatnagar, A.J. Bickley, H. Bindslev[14], J. Bizarro[21], S. Bliman[16], T. Bonicelli, S.J. Booth, G. Bosia, M. Botman, D. Boucher, H. Brelen, H. Brinkschulte, M. Brusati, T. Budd, M. Bures, T. Businaro, P. Butcher, H. Buttgereit, C. Caldwell-Nichols, D.J. Campbell, P. Card, G. Celentano, C.D. Challis, A. Cheetham, P. Chiron, J. Christiansen, C. Christodoulopoulos, P. Chuilon, R. Claesen, S. Clement[28], E. Clipsham, J.P. Coad, S. Conroy[12], M. Cooke, S. Cooper, J.G. Cordey, W. Core, G. Corrigan, S. Corti, A.E. Costley, G. Cottrell, J. Coulon[16], M. Cox[7], P. Cripwell[12], H. de Blank[15], G. Decker[32], H. de Esch, L. de Kock, E. Deksnis, G.B. Denne, G. Deschamps, G. Devillers, K.J. Dietz, J. Dobbing, N. Dolgetta, S.E. Dorling, P.G. Doyle, D.F. Düchs, H. Duquenoy, A. Edwards, J. Ehrenberg, T. Elevant[11], S.K. Erents[7], L.G. Eriksson[5], H. Fajemirokun[12], H. Falter, D. Flory, M. Forrest[7], J. Freiling[15], C. Froger, P. Froissard, K. Fullard, M. Gadeberg, A. Galetsas, M. Galley, M. Garribba, P. Gaze, X. Ge[25], R. Giannella, A. Gibson, R.D. Gill, A. Gondhalekar, C. Gormezano, N.A. Gottardi, C. Gowers, B.J. Green, W.K. Guo[25], R. Haange, G. Hammett[6], C.J. Hancock, P.J. Harbour, N.C. Hawkes[7], P. Haynes[7], J.L. Hemmerich, R. Hemsworth, F.B. Herzog, R.F. Herzog, J. Hoekzema, R. Hope, J. How, M. Huart, T.P. Hughes[30], M. Hugon, M. Huguet, A. Hwang[7], C. Idelon, B. Ingram, M. Irving, J. Jacquinot, H. Jaeckel, G. Janeschitz[13], O.N. Jarvis, F. Jensen, E.M. Jones, L.P.D.F. Jones, T.T.C. Jones, A. Kaye, B.E. Keen, M. Keilhacker, G.J. Kelly, W. Kerner, R. Konig, A. Konstantellos, M. Kovanen[20], P. Kupschus, P. Lallia, R. Lässer, J.R. Last, B. Laundy, L. Lauro-Taroni, K. Lawson[7], E. Lazzaro, M. Lennholm, P. Lomas, M. Lorentz-Gottardi[2], M. Loughlin, C. Lowry, B. Macklin, G. Maddison[7], G. Magyar, W. Mandl[13], V. Marchese, F. Marcus, J. Mart, E. Martin, R. Martin-Solis[31], P. Massmann, K.F. Mast[13], G. McCracken[7], P. Meriguet, S.F. Mills, P. Millward, S.L. Milora[23], E. Minardi[31], A. Moissonnier, F. Mompean, P.L. Mondino, F. Montvai[3], P. Morgan, H. Morsi, G. Murphy, M. Mynarends, C. Nardone, F. Nave[21], G. Newbert, M. Newman, P. Nielsen, P. Noll, W. Obert, D. O'Brien, J. O'Rourke, R. Ostrom, M.G. Pacco-Düchs, M. Pain, F. Paoletti, S. Papastergiou, D. Pasini, A. Peacock, N. Peacock[7], D. Pearson[12], C. Perry, V. Phillips[28], M. Pick, J. Plancoulaine, J-P. Poffé, F. Porcelli, L. Porte[19], R. Prentice, G. Radford[9], T. Raimondi, C. Raymond, P-H. Rebut, R. Reichle[13], J. Removille, G. Rey[16], F. Rimini, D. Robinson[7], A. Rolfe, R. Romain, R.T. Ross, L. Rossi, P. Rutter, H.C. Sack, G. Sadler, G. Saibene, N. Salmon[12], G. Sanazzaro, A. Santagiustina, R. Sartori, C. Sborchia, P.H. Schild, M. Schmid, G. Schmidt[6], S.M. Scott, A. Sibley, R. Simonini, A. Sips[15], P. Smeulders, S. Sommers, K. Sonnenberg, R. Stankiewicz[27], M. Stamp, P. Stangeby[18], D.F. Start, C.A. Steed, D. Stork, P.E. Stott, T.E. Stringer, D. Stubberfield, D. Summers, H. Summers[19], H. Tamnen, A. Tanga, A. Taroni, A. Tesini, P.R. Thomas, E. Thompson, K. Thomsen, J.M. Todd, P. Trevalion, B. Tubbing, F. Tibone, E. Usselmann, A. Vannucci, H. van der Beken, G. Vlases, M. von Hellermann, T. Wade, C. Walker, Z. Wang[26], D. Ward, M.L. Watkins, M.J. Watson, H. Weisen[10], J. Wesson, J. Wilks, U. Willen[11], D. Wilson, T. Winkel, S. Wolfe, B. Wolle[24], D. Wong, C. Woodward, M. Wykes, I.D. Young, L. Zannelli, Z. Zheng[25], Y. Zhu[26], M. Zouhar.

PERMANENT ADDRESS

1. UKAEA, Harwell, Didcot, Oxon. UK.
2. EUR-EB Association, LPP-ERM/KMS, B-1040 Brussels, Belgium.
3. Central Research Institute for Physics, Academy of Sciences, Budapest, Hungary.
4. ENEA-CENTRO Di Frascati, I-00044 Frascati, Roma, Italy.
5. Chalmers University of Technology, Göteborg, Sweden.
6. Princeton Plasma Physics Laboratory, New Jersey, USA.
7. UKAEA Culham Laboratory, Abingdon, Oxfordshire, UK.
8. Plasma Physics Laboratory, Space Research Institute, Sao José dos Campos, Brazil.
9. Institute of Mathematics, University of Oxford, UK
10. CRPP/EPFL, 21 Avenue des Bains, CH-1007 Lausanne, Switzerland.
11. Swedish Energy Research Commission, S-10072 Stockholm, Sweden.
12. Imperial College of Science and Technology, University of London, UK.
13. Max Planck Institut für Plasmaphysik, D-8046 Garching bei Munchen, FRG.
14. Risø National Laboratory, Denmark.
15. FOM Instituut voor Plasmafysica, 3430 Be Nieuwegein, The Netherlands.
16. Commissiariat à L'Énergie Atomique, Cadarache, F-13108 St Paul Lez Durance, France.
17. JAERI, Tokai Research Establishment, Tokai-Mura, Naka-Gun, Japan.
18. Institute for Aerospace Studies, University of Toronto, Downsview, Ontario, Canada.
19. University of Strathclyde, 107 Rottenrow, Glasgow, G4 0NG, UK.
20. Nuclear Engineering Laboratory, Lapeenranta University, Finland.
21. JNICT, Lisboa, Portugal.
22. CNP, Milan, Italy.
23. Oak Ridge National Laboratory, Oak Ridge, Tenn., USA.
24. University of Heidelberg, Heidelberg, FRG.
25. IPP, Academia Sinica, Beijing, P.R. China.
26. Southwestern Institute of Physics, Leshan, Sechuan, P.R. China.
27. RCC Cyfronet, Otwock Swierk, Poland.
28. Kernforschungsanlage, Jülich, FRG.
29. University of Leicester, Leicester, UK.
30. University of Essex, Colchester, UK.
31. Universidad Complutense de Madrid, Spain.
32. University of Dusseldorf, FRG.

J CR 88 156.5 (rev. 18/1/90)